JACS
JOURNAL OF THE AMERICAN CHEMICAL SOCIETY
pubs.acs.org/JACS
Article

Direct Observation of Covalently Bound Clusters in Resonantly Stabilized Radical Reactions and Implications for Carbonaceous Particle Growth

Hong Wang, Jiwen Guan,* Jiao Gao, Jinyang Zhang, Qiang Xu, Guangxian Xu, Ling Jiang, Lili Xing, Donald G. Truhlar,* and Zhandong Wang*

Cite This: J. Am. Chem. Soc. 2024, 146, 13571−13579

ABSTRACT: Based on quantum mechanically guided experiments that observed elusive intermediates in the domain of inception that lies between large molecules and soot particles, we provide a new mechanism for the formation of carbonaceous particles from gas-phase molecular precursors. We investigated the clustering behavior of resonantly stabilized radicals (RSRs) and their interactions with unsaturated hydrocarbons through a combination of gas-phase reaction experiments and theoretical calculations. Our research directly observed a sequence of covalently bound clusters (CBCs) as key intermediates in the evolution from small RSRs, such as benzyl (C_7H_7), indenyl (C_9H_7), 1-methylnaphthyl (1-$C_{11}H_9$), and 2-methylnaphthyl (2-$C_{11}H_9$), to large polycyclic aromatic hydrocarbons (PAHs) consisting of 28 to 55 carbons. We found that hydrogen abstraction and RSR addition drive the formation and growth of CBCs, leading to progressive H-losses, the generation of large PAHs and PAH radicals, and the formation of white smoke (incipient carbonaceous particles). This mechanism of progressive H-losses from CBCs (PHLCBC) elucidates the crucial relationship among RSRs, CBCs, and PAHs, and this study provides an unprecedentedly seamless path of observed assembly from small RSRs to large nanoparticles. Understanding the PHLCBC mechanism over a wide temperature range may enhance the accuracy of multiscale models of soot formation, guide the synthesis of carbonaceous nanomaterials, and deepen our understanding of the origin and evolution of carbon within our galaxy.

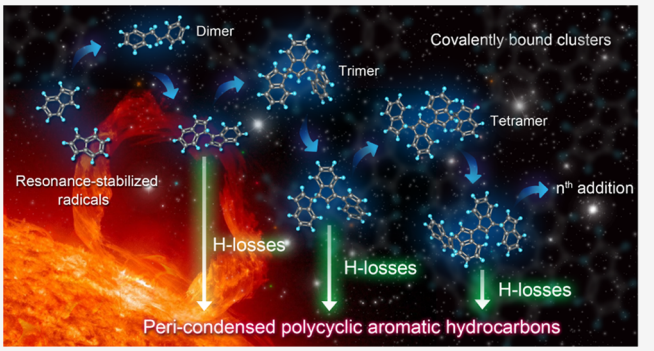

INTRODUCTION

The evolution of small precursor molecules into large polycyclic aromatic hydrocarbons (PAHs) is a topic of sustained interest in nanoparticle material synthesis, interstellar evolution, pyrolysis, and combustion. PAHs have been identified as crucial reaction intermediates in molecular mass-growth processes, leading to nanotubes and fullerenes. For instance, C_{60} and C_{70} were observed in pyrolysis and flame soot.[1−3] Graphene and carbon nanotubes are primarily composed of large PAHs, and they are promising materials for future capacitors, sensors, and transistors.[4,5] Beyond the Earth, aromatic structures have been proposed as potential carriers of the diffuse interstellar bands and unidentified infrared bands in extraterrestrial environments, such as circumstellar envelopes of carbon-rich stars;[6,7] PAHs are believed to contribute up to 30% of the interstellar carbon budget and have been associated with the prebiotic evolution of the interstellar medium.[8,9] Understanding the formation of PAHs in combustion environments is driven by the crucial role they play in producing environmentally hazardous soot particles from incomplete combustion processes,[10,11] which can have detrimental effects on human health, including an increased risk of cancer and respiratory illnesses.[12,13] Despite their significance, the understanding of the possible mechanisms of molecular weight growth processes of PAHs from small precursor molecules is incomplete.

The hydrogen-abstraction/acetylene-addition (HACA) mechanism, involving stepwise addition of C_2H_2 to an aromatic hydrocarbon radical, was the first "bottom-up" mechanism proposed to explain the molecular weight growth of most PAHs, especially under high-temperature combustion conditions.[14−17] Other small-molecule and radical-addition mechanisms have also been reported as alternative ways to understand PAH formation in high-temperature combustion and low-temperature interstellar environments.[18,19] Experiments have demonstrated hydrocarbon mass growth via

Received: March 8, 2024
Revised: April 18, 2024
Accepted: April 19, 2024
Published: May 6, 2024

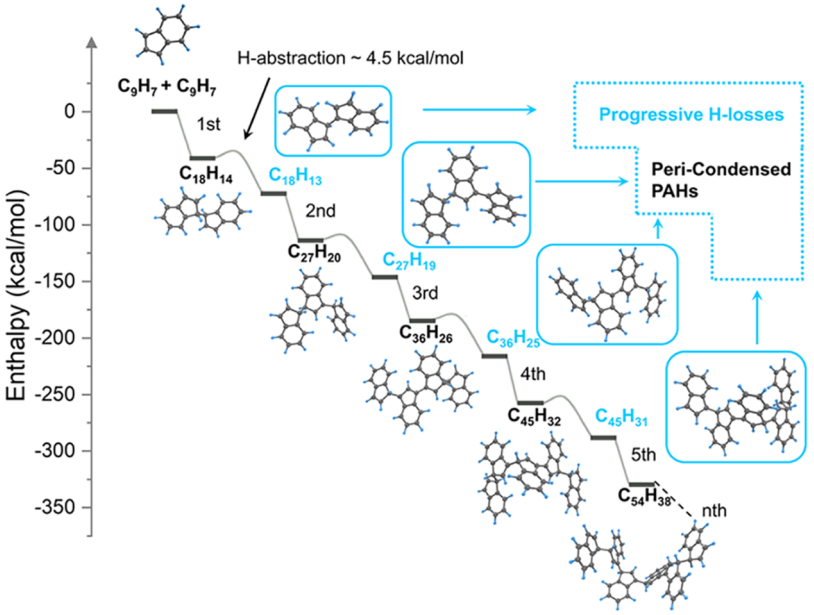

Figure 1. Calculated reaction pathway for repetitive H-abstractions and $^{\bullet}C_9H_7$ additions. Abstraction steps, enthalpy changes, and barriers are evaluated with H as the abstracting radical. The total number of H atoms is identical for all of the calculated enthalpies, but only active species involved during the H-abstraction reactions are shown in the figure. The ordinal numbers denote the number of $^{\bullet}C_9H_7$ additions. The blue arrows suggest the formation of peri-condensed PAHs via progressive H-losses (discussed in the text).

hydrogen abstraction-vinylacetylene (C_4H_4) addition (HAVA)[20−22] and phenyl-addition dehydrocyclization (PAC).[23] A kinetic modeling study indicated a slow efficiency of stepwise C_2H_2/C_4H_4 addition to reproduce the observed PAH concentrations in flame experiments.[24] The mass growth of PAH and soot in the absence of hydrogen radicals suggests that these documented pathways may not be favorable in radical-deficient environments as many free radicals are required for the activation of stable PAH molecules in the HACA, HAVA, and PAC mechanisms.[25] In addition, distinct aromatics such as peri-condensed aromatic hydrocarbons,[26] cata-condensed and pentagonal-ring linked species,[27] and bridged aromatics linked by aliphatic chains[28] have been suggested in flames and soot. However, the existing mechanisms do not fully explain the formation behavior of PAHs in various environments.

Localized π-radicals, also known as resonance stabilized radicals (RSRs), have been directly detected in nascent soot from flames,[29] hydrocarbon pyrolysis,[30,31] and even in the cold molecular cloud TMC-1.[32] RSR can accumulate in reactive environments and contribute to the formation of PAHs and soot. The discovery of RSRs in a combustion environment may imply an unknown mechanism of soot inception. Johansson et al. proposed clustering of hydrocarbons by radical chain reactions (CHRCR) as an important pathway for soot inception[33] by proposing that PAHs form without depleting the radical pool through RSR chain reactions, where radical−radical recombination is followed by immediate H atom ejection to form a new RSR. The prompt H loss in CHRCR allows sequential growth without requiring reactivation through H-abstraction reactions. Despite the promising potential of radical chain reactions for rapid hydrocarbon growth, there is a lack of research investigating the role of RSR radical−radical chain reactions in the molecular weight growth of PAHs.[34] Using a microreactor, researchers have concentrated on the investigations of radical−radical recombination reactions,[35−38] revealing the formation of prototypical PAHs such as tricyclic phenanthrene ($C_{14}H_{10}$) and tetracyclic pyrene ($C_{16}H_{10}$).

Understanding the role of RSR and elucidating the molecular weight growth processes via radical chain reactions in the combustion or pyrolysis of hydrocarbon fuels are challenging due to the involvement of numerous reactive species. In this work, we chose to pyrolyze halogenated radical precursors in a laminar flow reactor, where RSR is exclusively produced via cleavage of the C−Br bond at a high temperature. The clean environment permits better assessment of the RSR-involved radical chain reactions, unlike the "dirty" combustion or pyrolysis. By preparing typical RSRs such as benzyl (C_7H_7), indenyl (C_9H_7) 1-methylnaphthyl (1-$C_{11}H_9$), and 2-methylnaphthyl (2-$C_{11}H_9$), and examining their reactivity under the pyrolytic condition, we find that the obtained array of data consistently reveals a previously unseen and smooth progression from small RSRs to much larger PAHs consisting of C_{28}−C_{55} carbons. A sequence of covalently bound clusters (CBCs) is directly observed as the key intermediate species that bridges the gap between the small RSRs and the large PAHs. Hydrogen abstraction and RSR addition drive the rapid formation and growth of CBCs, which undergo progressive H-losses and evolve into large PAHs and large PAH radicals. We hence propose a mechanism of progressive H-losses from CBCs (abbreviated as PHLCBC), to explain the crucial "golden triangle" relationship among RSR, CBC, and PAH. Recognition of the PHLCBC mechanism may enhance the fidelity and accuracy of multiscale models of soot inception, guide the synthesis of carbonaceous nanomaterials, and further deepen our understanding of the origin and evolution of carbon within our galaxy.

RESULTS AND DISCUSSION

Recent flame experiments have indicated that benzyl is a significant precursor of various aromatic hydrocarbons.[39]

https://doi.org/10.1021/jacs.4c03417
J. Am. Chem. Soc. 2024, 146, 13571−13579

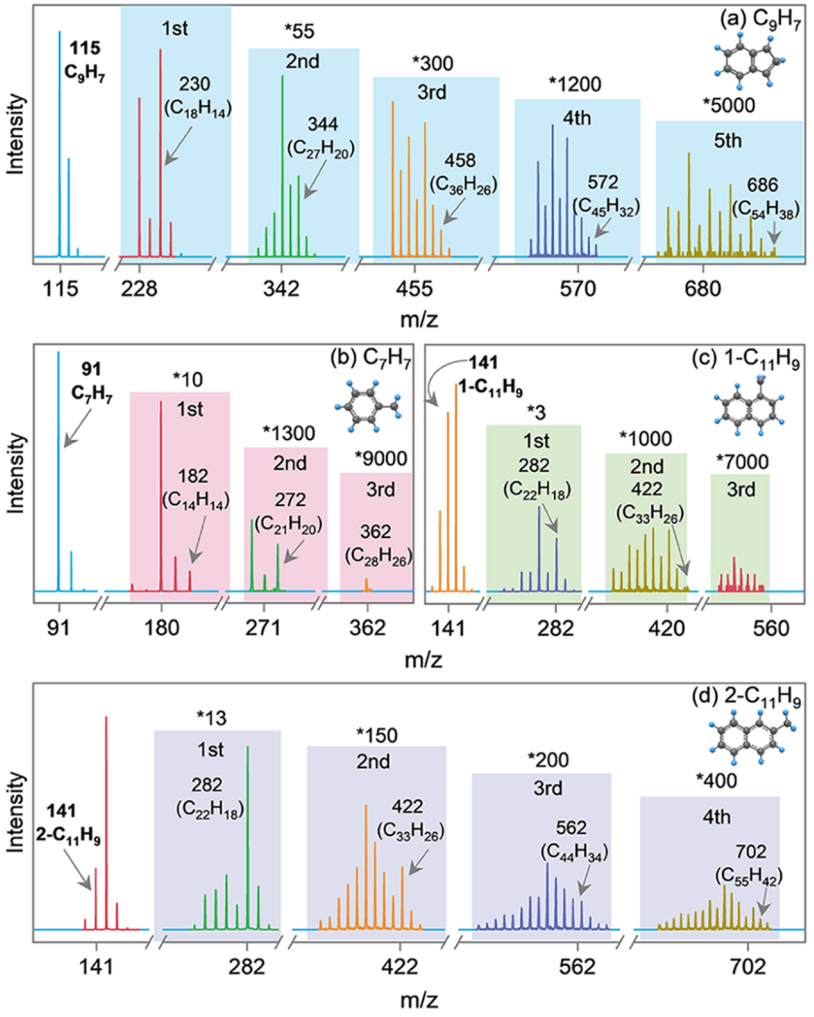

Figure 2. SVUV-PIMS mass spectra of products from the pyrolysis of selected precursors in a flow reactor at a pressure of 20 mbar. (a) 2-Bromoindene (C_9H_7Br) at 800 K and 9.5 eV, (b) benzyl bromide (C_7H_7Br) at 800 K and 10.0 eV, (c) 1-bromomethyl naphthalene (1-$C_{11}H_9Br$) at 1100 K and 10.5 eV, and (d) 2-bromomethyl naphthalene (2-$C_{11}H_9Br$) at 1100 K and 10.5 eV. The photon energy is tuned to avoid the interference of photodissociation. The mass peaks of RSRs and CBCs are labeled with their molecular formula. Factors are applied to better visualize the mass peaks and are indicated in the figure.

Dimerization of benzyl was one of the most fundamental reactions to generate phenanthrene ($C_{14}H_{10}$) consisting of three fused benzene rings.[35] Indenyl (C_9H_7), a key RSR with a cyclopenta-fused bicyclic structure, and the dimerization of 1-Indenyl (1-C_9H_7) can form chrysene ($C_{18}H_{12}$).[40] By the pyrolysis of indene (C_9H_8), and a mixture of ethylene with a small amount of indene, Rundel et al. found that indenyl can promote the soot particle formation.[30] Hence, the dimerization of benzyl and indenyl radical are experimentally validated processes, and additionally, PAH dimers stabilized through the formation of covalent bonds have recently been evidenced in the study of a laminar diffusion methane flame.[41]

RSR Additions to Form CBCs: Dimerization and Polymerization Processes of RSRs by Radical Chain Reaction. First, we investigate the potential energy surfaces (PESs) of benzyl and indenyl clustering. Figure 1 shows a quantum mechanical reaction pathway for a mechanism with repeated H-abstractions and indenyl ($^{\bullet}C_9H_7$) additions (see the Computational Methodssection). Barrierless self-recombination of 1-indenyl radicals gives diindene (the $C_{18}H_{14}$ reactive dimer). Then, H-abstraction of $C_{18}H_{14}$ forms a $^{\bullet}C_{18}H_{13}$ radical with a forward barrier of ~4.5 kcal/mol. This new RSR can either undergo another $^{\bullet}C_9H_7$ addition to produce $C_{27}H_{20}$ (trimer) or undergo progressive H-losses to produce the stable benzenoid $C_{18}H_{12}$ (a PAH discussed below). Then, H-abstraction and $^{\bullet}C_9H_7$-addition steps can be repeated to form much larger CBCs and RSRs, e.g., $C_{36}H_{26}$, $^{\bullet}C_{36}H_{25}$, $C_{45}H_{32}$, $^{\bullet}C_{45}H_{31}$, $C_{54}H_{38}$, and so forth. The overall reaction is exothermic, and consequently, the formation of CBCs is expected to be highly efficient. A similar mechanistic step is also calculated to be feasible for repetitive H-abstraction and benzyl ($^{\bullet}C_7H_7$) addition (Figure S1).

To generate the reaction sequence predicted by theory, we pyrolyzed a controlled mixture of RSR precursors in a laminar flow reactor. A sequence of CBCs is observed by using in situ synchrotron radiation ultraviolet photoionization mass spectrometry (SVUV-PIMS) (see the Experimental Methods section and Figure S2). Figure 2a shows the mass spectra (as mass/charge ratio m/z in Da) of the products from the pyrolysis of 2-bromoindene (C_9H_7Br) at 800 K. The mass signal at m/z = 115 is identified as the 1-indenyl radical (discussed below). Self-recombination of 1-indenyl produces diindene $C_{18}H_{14}$ (dimer) at 230. The signal at m/z = 229 is attributed to a radical intermediate $^{\bullet}C_{18}H_{13}$ formed from the

https://doi.org/10.1021/jacs.4c03417
J. Am. Chem. Soc. 2024, 146, 13571−13579

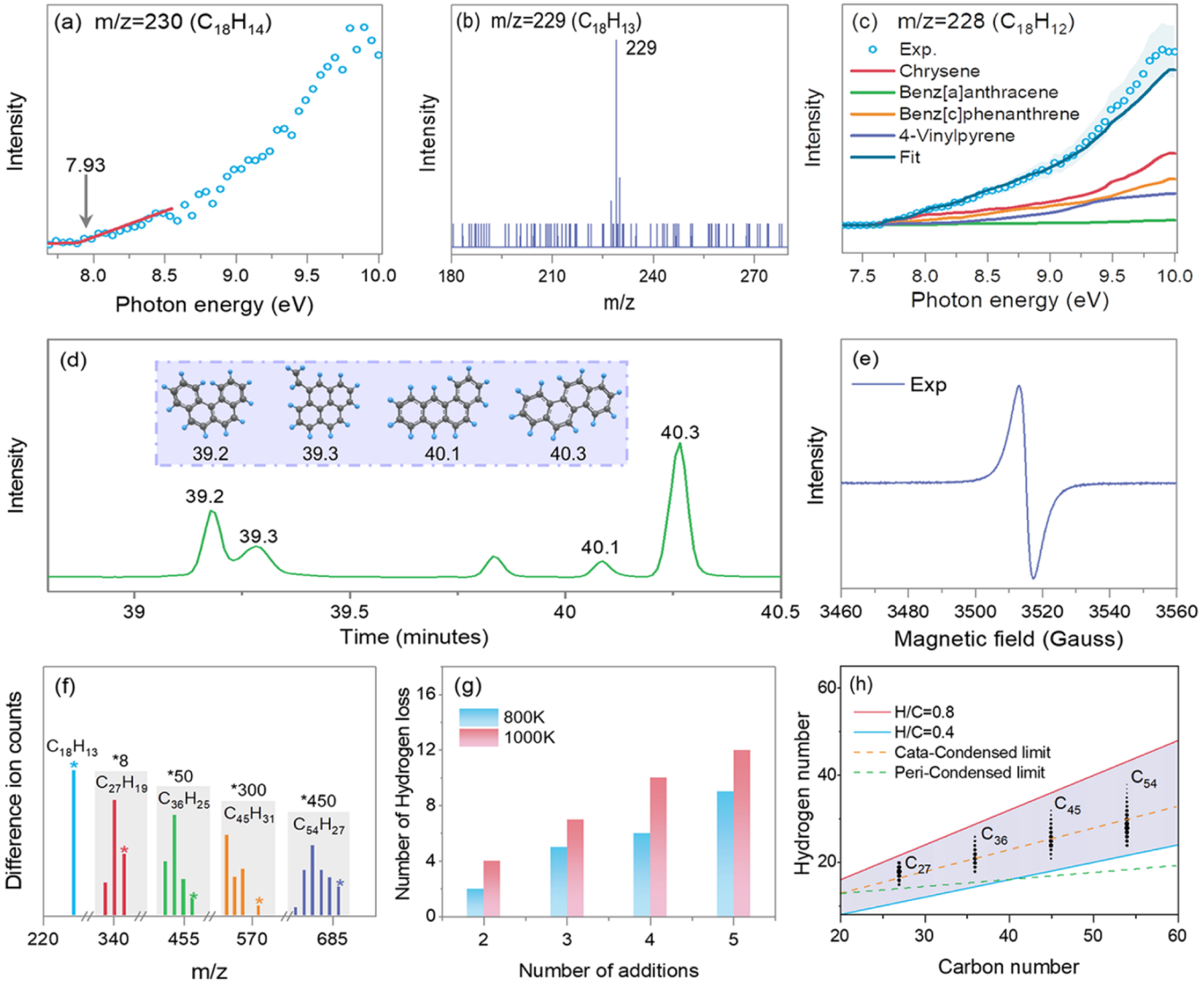

Figure 3. Product identification of indenyl radical reactions. (a) PIE curves of m/z = 230 from the pyrolysis of 2-bromoindene (C_9H_7Br) in a flow reactor (800 K and 4 mbar), (b) photoionization mass spectrum of m/z = 229 at 7.0 eV, and (c) PIE of m/z = 228. (d) GC-MS spectrum of the enrichment products in the C_9H_7Br pyrolysis. The inset shows structures and the retention times of the standard $C_{18}H_{12}$ samples. (e) EPR spectrum of the enriched products in C_9H_7Br pyrolysis. (f) Difference ion intensity of the measured C_xH_y products with the odd number of hydrogen atoms after subtracting (see text) the ^{13}C contributions. (g) The number of H-losses from the parent clusters. (h) Black dots are the C_xH_y distribution of the measured PAH products at 1000 K. The shaded area corresponds to an H/C ratio of 0.4−0.8. The empirical limits of cata-condensed (dashed line) and peri-condensed (dotted line) PAHs are also shown.

H-abstraction of $C_{18}H_{14}$. A second $^{\bullet}C_9H_7$ addition on $C_{18}H_{13}$ forming $C_{27}H_{20}$ (trimer) is evidenced by the signal at 344. The series of tetramer ($C_{36}H_{26}$) at 458, pentamer ($C_{45}H_{32}$) at 572, and hexamer ($C_{54}H_{38}$) at 686 demonstrate the consecutive H-losses and five stepwise additions. The earlier aerosol experiments by Rundel et al. have also detected the indenyl dimer and trimer as the chemical composition of the soot particle from indene pyrolysis,[30] implying the probable roles of the clusters for soot formation. Figure 2b−d shows the mass spectra of the products from reactions of benzyl ($^{\bullet}C_7H_7$), 1-methylnaphthyl ($^{\bullet}1$-$C_{11}H_9$), and 2-methylnaphthyl ($^{\bullet}2$-$C_{11}H_9$), respectively. The $^{\bullet}C_7H_7$ reaction leads to three successive benzyl-radical additions forming dimer ($C_{14}H_{14}$), trimer ($C_{21}H_{20}$), and tetramer ($C_{28}H_{26}$). Analogously, the mass spectrum of 1-methylnaphthyl reactions reveals three successive $^{\bullet}C_{11}H_9$ radical additions forming dimer ($C_{22}H_{18}$), trimer ($C_{33}H_{26}$), and tetramer ($C_{44}H_{34}$), and the mass spectrum of 2-methylnaphthyl reveals four successive $^{\bullet}C_{11}H_9$ radical additions to dimer ($C_{22}H_{18}$), trimer ($C_{33}H_{26}$), tetramer ($C_{44}H_{34}$), and pentamer ($C_{55}H_{42}$).

To evaluate the significance of the CBCs under combustion-like conditions, we pyrolyzed indene (a practical fuel) at 1300 K and ambient pressure in a laminar flow reactor. The matrix-assisted laser desorption/ionization mass spectrometry (MALDI-MS) was used to analyze the pyrolytic products. Although there are many mass peaks associated with the pyrolytic and mass growth products of indene, Figure S3 clearly shows a sequence of mass peaks associated with the covalent bound clusters formed through the six consecutive H-abstraction and C_9H_7 addition and the progressive H-loss products, and the clusters of C_{18}−C_{63} remain prevalent in the indene pyrolysis.

Clustering of stable unsaturated hydrocarbons such as benzene (C_6H_6), naphthalene ($C_{10}H_8$), and phenanthrene

https://doi.org/10.1021/jacs.4c03417
J. Am. Chem. Soc. 2024, 146, 13571−13579

($C_{14}H_{10}$) with RSRs ($^{\bullet}C_9H_7$, $^{\bullet}C_7H_7$) is also examined in this work because most of the carbon is in the form of stable closed-shell species. Under the same conditions, only one RSR can be added to the stable unsaturated hydrocarbon, and its signal intensity is much lower than the product of RSR dimerization. We find that the clustering of these stable unsaturated hydrocarbons with RSRs is much less favorable than the RSR−RSR clustering, elevating the significance of RSR−RSR clustering under our experimental conditions. The representative mass spectra are shown in Figure S4.

Progressive H-Loss of CBCs. Figure 2a−d also reveals that CBCs can undergo progressive H-loss reactions. For each cluster, many mass peaks with successive mass decrements of 1 Da are observed, and they are interpreted as radical intermediates and stable PAHs. To allow a dominant production of the indenyl dimer and a focus on its progressive H-loss reaction pathways, a lower pressure of 4 mbar (3 Torr) was used for the pyrolysis of C_9H_7Br. At this pressure, we detect mass peaks 115, 230, 229, and 228 (Figure S5), which are consistent with the measured ones in Figure 2a. The photoionization efficiency (PIE) curve at m/z = 115 in Figure S6 is consistent with the production of 1-indenyl. Figures 2a and S5 reveal that self-recombination of 1-indenyl forms 1,1-diindene $C_{18}H_{14}$ (dimer). The calculated ionization energy (IE) of 1,1-diindene is 7.98 eV, which agrees with the measured IE in Figure 3a. Mass peak 229 corresponds to $C_{18}H_{13}$, which could be a radical intermediate $^{\bullet}C_{18}H_{13}$ or an isotope of $^{13}C^{12}C_{17}H_{12}$ (with natural abundance). The calculated IE of $^{\bullet}C_{18}H_{13}$ is 6.91 eV. At 7.00 eV, the absence of 228 and the presence of 229 (Figure 3b) confirm the existence of this key radical intermediate.

The experimental PIE of 228 ($C_{18}H_{12}$) in Figure 3c can be well fit with a linear combination of the reference PIEs of chrysene, benz[*a*]anthracene, benz[*c*]phenanthracene, and 4-vinylpyrene.[20,22] The isomeric composition with a molecular weight of 228 is further revealed by gas chromatography−mass spectrometry (GC-MS) in Figure 3d (see the Experimental Methods section and Figure S7); these GC peaks are consistent with the ones measured from the standard samples of benz[*c*]phenanthracene, 4-vinylpyrene, benz[*a*]anthracene, and chrysene listed in the figure. The GC-MS results support the conclusion of the PIE analysis. The formation pathways of the observed dimeric products are further elucidated by quantum mechanical calculations on $C_{18}H_{14}$, $^{\bullet}C_{18}H_{13}$, $C_{18}H_{12}$, and the corresponding transition states (Figure S8 and the corresponding discussion). The main processes are H-abstraction of $C_{18}H_{14}$ to produce $^{\bullet}C_{18}H_{13}$ followed by dehydrocyclization reactions of this radical intermediate leading to the measured $C_{18}H_{12}$ isomers. In these processes, the two cyclopentadienyl moieties of the dimer are converted to six-membered ring structures.

Considered together, the spectra in Figures 2 and 3a−d demonstrate the interesting sequence of CBCs formed by RSR clustering. They identify the $C_{18}H_{14}$, $C_{18}H_{13}$ intermediates, and isomeric $C_{18}H_{12}$ PAH products from the C_9H_7 dimerization reaction, and the mechanism of CBCs formed via repetitive H-abstraction and RSR addition is experimentally confirmed.

Formation of Large PAHs and PAH Radicals. The radical intermediates are formed not only by H-loss from the dimer but also by progressive H-losses of larger clusters. Because the mass spectral signals of the radical species in Figure 2a might be adulterated by ^{13}C isotopes, we examine the presence of radicals by electron paramagnetic resonance (EPR) spectroscopy. Figures 3e and S9 show the EPR spectra of the enriched pyrolysis products of the four systems. With the measured resonance frequency of the single peak in Figures 3e and S9, the calculated Landé *g*-factors are all equal to 2.0033, which is very close to the value of free electrons (2.0023), suggesting that the enriched products contain persistent carbon-centered aromatic radicals where the unpaired electron has very little orbital contribution to the magnetic moment. The assignment is consistent with the previous EPR assignment from the sampled products of the laminar premixed ethylene and ethylene-benzene flames.[42] These radicals in the enriched products might be large and inert PAH radicals that have long lifetimes. In addition, by subtracting the calculated ion contributions of the corresponding isotopes (with natural abundance intensity), we confirm ion intensities with an odd number of hydrogen atoms attributed to radicals in Figure 3f. These ion intensities provide further evidence for the series of radical intermediates formed from the progressive H-losses of the CBCs.

The evolution processes of the H-losses are sensitive to the temperature and the size of the CBCs. Figure 3g presents the number—as counted from the corresponding SVUV-PIMS mass spectra (Figure S10(a))—of H-losses for each cluster size formed by $^{\bullet}C_9H_7$ reactions. This panel shows that the number of H-losses increases with the size of the cluster and with the temperature. Progressive H-losses are also observed in the other RSR reaction systems (Figure S10b,d), where the aliphatically bridged PAHs are the initial products. Figure S10(b−d) demonstrates that H atoms are progressively lost from each aliphatically bridged PAH cluster. Our results consistently reveal that the larger CBCs lose H atoms readily, especially at higher temperatures. The chemical evolution from CBCs to peri-condensed PAHs is expected to be extensive with the increase in temperature.

The progressive H-losses of CBCs form a sequence of PAH radicals and PAHs. The PAH growth by this mechanism is denoted as progressive hydrogen loss from CBCs (PHLCBC). The structural evolution of the large clusters is difficult to obtain from quantum mechanical calculations. By the SVUV-PIMS measurement, we also obtain the PIE curves of the intermediates from the indenyl trimerization, e.g., $C_{27}H_{20}$, $C_{27}H_{18}$. As shown in Figure S11(a), the ionization onset of $C_{27}H_{20}$ is determined at 7.4 ± 0.05 eV, the ionization onset of $C_{27}H_{18}$ is around 7.1 eV and the second onset is around 7.4 eV.

To demonstrate the complexity of resolving these isomers, we computationally constructed the possible isomeric structures of $C_{27}H_{20}$ and $C_{27}H_{18}$ and calculated their IEs. Figure S11(b) shows that the calculated IEs of the three $C_{27}H_{20}$ isomers (i1-1, i1-2, i1-3) are close to or slightly above the measured IE. For the $C_{27}H_{18}$, the calculated IE of i2-2 and i2-3 are close to the first ionization onset, and the IE of i2-1 is consistent with the second ionization onset. Thus, all of these isomers are possible intermediates. Extensive structural determinations of the larger clusters are challenging, but we follow previous works[43−45] where the observed *H*/*C* distributions are used to classify PAH structures as cata-condensed (a structure in which no carbon is shared by more than two rings) and peri-condensed (in which such sharing is present). Figure 3h shows the *H*/*C* plots of all products in the C_9H_7Br pyrolysis experiments, and *H*/*C* plots of the products in Figure 2b−d are shown in Figure S12(a−c). Figure 3h indicates that those products with the highest *H*/*C* ratios are cata-condensed. With progressive H-losses, each CBC evolves

https://doi.org/10.1021/jacs.4c03417
J. Am. Chem. Soc. 2024, 146, 13571−13579

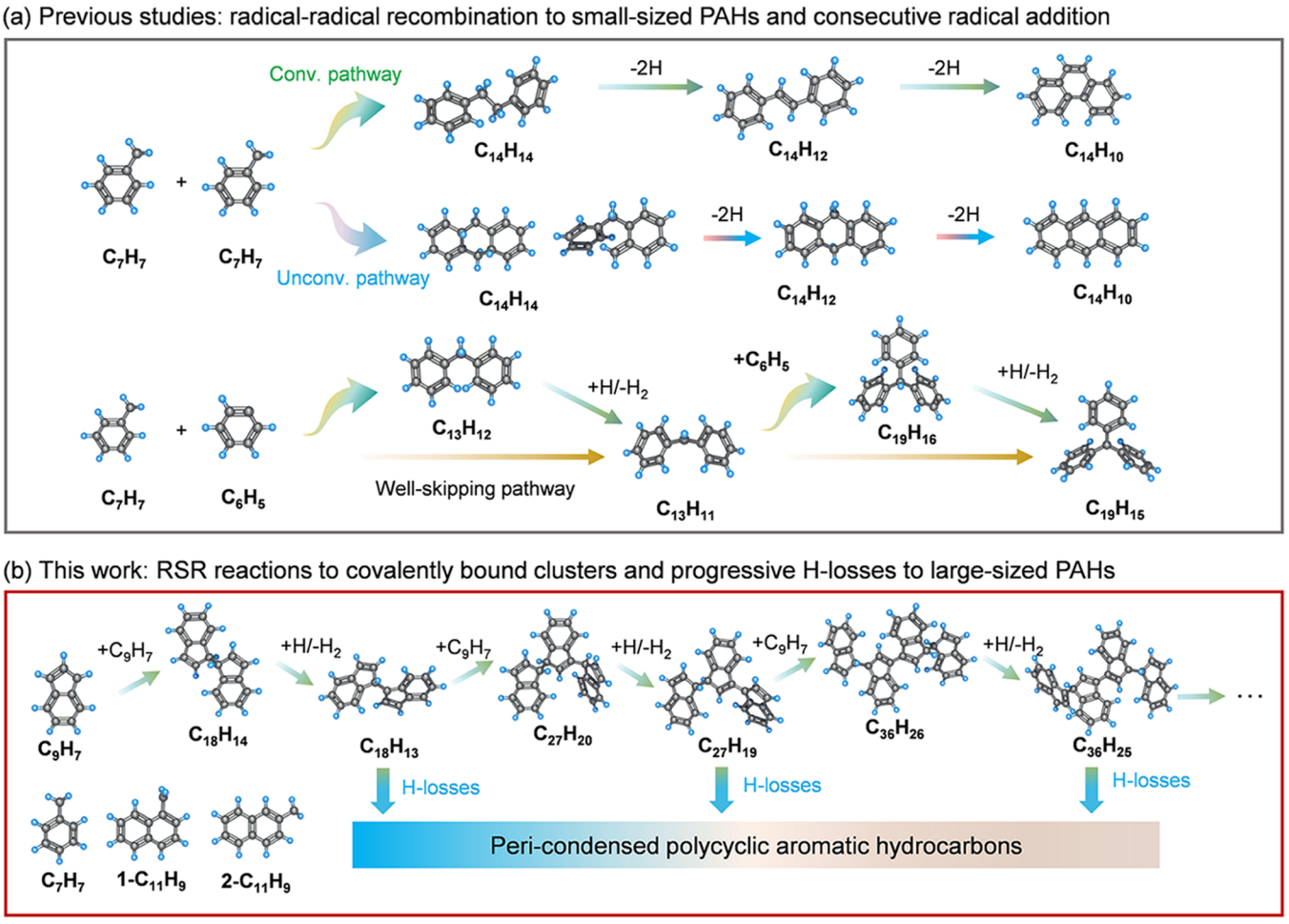

Figure 4. Comparison of the results of this work to previously reported mechanisms. (a) Previous studies: The conventional formation pathway of phenanthrene and the unconventional formation pathway of anthracene via C_7H_7 self-reaction; the reaction of C_7H_7 with consecutive two phenyl (C_6H_5) radical additions to form the $C_{13}H_{11}$ and $C_{19}H_{15}$ radical either by direct well-skipping pathway or the radical−radical association and subsequent H-abstraction pathway. (b) This work: the facile formation of CBCs growing in size by repetitive H-abstraction and RSR addition. The representative RSRs are C_9H_7, C_7H_7, 1-$C_{11}H_9$, and 2-$C_{11}H_9$. The pathway of progressive H-losses of CBCs leading to large-sized peri-condensed PAHs.

from the cata-condensed region of the plot toward the maximally peri-condensed limit, but none of them reach that limit or go beyond it, and thus, the final PAH products are a mixture of cata- and peri-condensed structures with six-membered rings. This is consistent with the calculated reaction pathways of the indenyl dimer, where two cyclopentadienyl moieties are converted to six-membered ring structures upon H-losses. In Figure S13, the conceivable structure evolutions of the $C_{27}H_{20}$ (trimer) and $C_{36}H_{26}$ (tetramer) to peri-condensed PAHs are provided, where the cyclopentadienyl moieties are progressively converted to six-membered ring structures.

In the previous studies,[35−38] the RSR−RSR recombination reactions have been carried out to learn the formation pathways of the prototypical PAHs. As shown in Figure 4a, phenanthrene was evidenced as the single $C_{14}H_{10}$ product in the experimental and computational studies of benzyl self-reaction.[35,37] Coupling a microreactor with the SVUV-PIMS, Kaiser et al. re-explored C_7H_7 self-reaction and identified a new $C_{14}H_{10}$ isomer anthracene.[36] They proposed unconventional pathways to explain the formation of anthracene.[36] Until recently, Couch et al. studied the C_6H_5 + C_7H_7 reaction and obtained the evidence of the diphenylmethyl ($C_{13}H_{11}$) radical from well-skipping H-loss (see Figure 4a);[34] the radical chain reaction continues when $C_{13}H_{11}$ associates with C_6H_5 to form triphenylmethane ($C_{19}H_{16}$) and triphenylmethyl ($C_{19}H_{15}$). In the present work, we directly observe a sequence of CBCs formed through consecutive H-abstraction and RSR addition (benzyl, indenyl, 1-methylnaphthyl, and 2-methylnaphthyl). Furthermore, the observation of the progressive H-loss of the CBCs (see the reaction scheme of Figure 4b) suggests the facile formation of very large PAHs with more-than-four-membered aromatic rings. Therefore, the PHLCBC mechanism proposed here further elucidates the crucial "golden triangle" relationship among RSRs, CBCs, and PAHs.

CONCLUSIONS

Note that the present studies are carried out over a limited temperature range, and it is probable that the dominant mechanism for PAH formation is not the same under all conditions, but the PHLCBC mechanism for PAH growth provided in this work is likely to be significant in many contexts. In a carbon-rich asymptotic giant branch star, carbonaceous dust formation occurs in an equilibrium zone characterized by low ionization and UV radiation. This carbonaceous dust evolves until it can be expelled into the interstellar medium. Although the specific conditions in the

https://doi.org/10.1021/jacs.4c03417
J. Am. Chem. Soc. 2024, 146, 13571−13579

nucleation zone are uncertain, the temperature is estimated to be ∼1000 K, and PAHs are hypothesized to form in these stellar envelopes.[46,47] In the pyrolysis of hydrocarbon fuels,[30,31] soot particle onset temperatures were observed in the range of 900−1150 K, which fits well the temperature range of the PHLCBC mechanism discovered in this work. A full recognition of PHCLBC over a wide temperature range can enhance the fidelity and accuracy of multiscale models of soot inception and nanomaterial synthesis, and it may further contribute to our understanding of the formation of interstellar PAHs and the origin and evolution of carbon within our galaxy.

METHODS

Computational Methods. All electronic structure calculations were performed using the Gaussian 16 program package.[48] The structures, energies, and harmonic zero-point energies of local minima and transition states were calculated by Kohn−Sham density functional theory with the global-hybrid MN15 exchange−correlation density functional and with the MG3S basis set.[49] The nature of the transition states was confirmed by the presence of an imaginary frequency for the reaction coordinate. Minimum energy paths (also called intrinsic reaction coordinates) were calculated to confirm connections between transition states and local or global minima. All energetic results are presented as enthalpies at 298 K; the enthalpy at 298 K equals the sum of the potential energy (electronic energy, including nuclear repulsion) and the zero-point vibrational energy.

Experimental Methods. The pyrolysis experiments were carried out using a customized flow reactor made of quartz coupled with the SVUV-PIMS at the BL09U beamline of the National Synchrotron Radiation Laboratory. Details of the BL09U beamline and the experimental setup of this work are described elsewhere (see the Supporting Information). Briefly, a continuous beam of radicals was prepared in situ through the pyrolysis of the selected halide precursor (see the sample information below) in the flow reactor. The temperature of the flow reactor can be tuned in the range of 300−1200 K. At the center of the flow reactor, a sampling cone with a 380 μm aperture was employed for molecular-beam sampling. The reactants and products in the flow reactor were expanded into a differential chamber (1.0×10^{-1} Pa) and passed through an orifice into the ionization chamber (1.0×10^{-3} Pa), where they were intersected and ionized by the quasi-continuous tunable synchrotron VUV light and immediately detected by the homemade reflectron time-of-flight mass spectrometer. Using this setup, the pyrolysis of 2-bromoindene C_9H_7Br (Macklin, purity ≥ 97%), benzyl bromide C_7H_7Br (Macklin, purity ≥ 98%), 1-bromomethyl naphthalene 1-$C_{11}H_9Br$ (Aladdin, purity ≥ 97%), and 2-bromomethyl naphthalene 2-$C_{11}H_9Br$ (Aladdin, purity ≥ 97%) were carried out at the pressure of 4 or 20 mbar. More details are described in Text S1. GC-MS, EPR, and MALDI-MS are used to study the PAH formation from the RSR reactions. The enriched procedures were implemented in these methods. The details of these experimental setups and experimental conditions are all provided in Text S1.

ASSOCIATED CONTENT

Supporting Information

The Supporting Information is available free of charge at https://pubs.acs.org/doi/10.1021/jacs.4c03417.

Additional experimental and computational details, and supporting figures (Figure S1−S13) and tables (Tables S1 and S2) as mentioned in the text (PDF)

AUTHOR INFORMATION

Corresponding Authors

Jiwen Guan − *National Synchrotron Radiation Laboratory, University of Science and Technology of China, Hefei 230029 Anhui, P. R. China*; Email: jguan43@ustc.edu.cn

Donald G. Truhlar − *Department of Chemistry, Chemical Theory Center, and Minnesota Supercomputing Institute, University of Minnesota, Minneapolis, Minnesota 55455-0431, United States*; orcid.org/0000-0002-7742-7294; Email: truhlar@umn.edu

Zhandong Wang − *National Synchrotron Radiation Laboratory, University of Science and Technology of China, Hefei 230029 Anhui, P. R. China; State Key Laboratory of Fire Science, University of Science and Technology of China, Hefei 230026 Anhui, P. R. China*; orcid.org/0000-0003-1535-2319; Email: zhdwang@ustc.edu.cn

Authors

Hong Wang − *National Synchrotron Radiation Laboratory, University of Science and Technology of China, Hefei 230029 Anhui, P. R. China*

Jiao Gao − *Dalian Institute of Chemical Physics, Chinese Academy of Sciences, Dalian 116023, P. R. China*

Jinyang Zhang − *National Synchrotron Radiation Laboratory, University of Science and Technology of China, Hefei 230029 Anhui, P. R. China*

Qiang Xu − *National Synchrotron Radiation Laboratory, University of Science and Technology of China, Hefei 230029 Anhui, P. R. China*

Guangxian Xu − *National Synchrotron Radiation Laboratory, University of Science and Technology of China, Hefei 230029 Anhui, P. R. China*

Ling Jiang − *Dalian Institute of Chemical Physics, Chinese Academy of Sciences, Dalian 116023, P. R. China*; orcid.org/0000-0002-8485-8893

Lili Xing − *Energy and Power Engineering Institute, Henan University of Science and Technology, Luoyang 471003 Henan, P. R. China*; orcid.org/0000-0003-2099-8472

Complete contact information is available at: https://pubs.acs.org/10.1021/jacs.4c03417

Funding

National Key Research and Development Program of China (no. 2021YFA1601800); National Natural Science Foundation of China (no. GG2310000379); CAS Project for Young Scientists in Basic Research (no. YSBR-028); U.S. Department of Energy, Office of Science, Office of Basic Energy Sciences under Award DE-SC0015997 (DGT).

Notes

The authors declare no competing financial interest.

ACKNOWLEDGMENTS

The authors express their gratitude to Prof. Katharina Kohse-Höinghaus from Bielefeld University and Dr. Maurin Salamanca from Universidad Nacional de Colombia for providing valuable suggestions to improve the manuscript. EPR and MALDI-MS measurements were carried out at the Instruments Center for Physical Science, University of Science and Technology of China. This work was supported by National Key Research and Development Program of China (no. 2021YFA1601800), National Natural Science Foundation of China (no. GG2310000379), Chinese Academy of Sciences (CAS) Project for Young Scientists in Basic Research (no. YSBR-028), and U.S. Department of Energy, Office of Science, Office of Basic Energy Sciences under Award DE-SC0015997.

REFERENCES

(1) Homann, K. H. Fullerenes and soot formation - New pathways to large particles in flames. *Angew. Chem. Int. Ed.* **1998**, *37*, 2434−2451.

(2) Howard, J. B.; McKinnon, J. T.; Makarovsky, Y.; Lafleur, A. L.; Johnson, M. E. Fullerenes C_{60} and C_{70} in flames. *Nature* **1991**, *352*, 139−141.

(3) Taylor, R.; Langley, G. J.; Kroto, H. W.; Walton, D. R. Formation of C_{60} by pyrolysis of naphthalene. *Nature* **1993**, *366*, 728−731.

(4) Franklin, A. D.; Luisier, M.; Han, S. J.; Tulevski, G.; Breslin, C. M.; Gignac, L.; Lundstrom, M. S.; Haensch, W. Sub-10 nm carbon nanotube transistor. *Nano Lett.* **2012**, *12*, 758−762.

(5) Miller, J. R.; Outlaw, R. A.; Holloway, B. C. Graphene double-layer capacitor with ac line-filtering performance. *Science* **2010**, *329*, 1637−1639.

(6) Peeters, E.; Mackie, C.; Candian, A.; Tielens, A. A Spectroscopic view on cosmic PAH emission. *Acc. Chem. Res.* **2021**, *54*, 1921−1933.

(7) Schlemmer, S.; Cook, D. J.; Harrison, J. A.; Wurfel, B.; Chapman, W.; Saykally, R. J. The unidentified interstellar infrared bands: PAHs as carriers? *Science* **1994**, *265*, 1686−1689.

(8) Herbst, E.; van Dishoeck, E. F. Complex Organic Interstellar Molecules. *Annu. Rev. Astron. Astrophys.* **2009**, *47*, 427−480.

(9) Tielens, A. G. Interstellar polycyclic aromatic hydrocarbon molecules. *Annu. Rev. Astron. Astrophys.* **2008**, *46*, 289−337.

(10) Martin, J. W.; Salamanca, M.; Kraft, M. Soot inception: Carbonaceous nanoparticle formation in flames. *Prog. Energy Combust. Sci.* **2022**, *88*, No. 100956.

(11) Richter, H.; Howard, J. B. Formation of polycyclic aromatic hydrocarbons and their growth to soot−A review of chemical reaction pathways. *Prog. Energy Combust. Sci.* **2000**, *26*, 565−608.

(12) Agudelo-Castañeda, D. M.; Teixeira, E. C.; Schneider, I. L.; Lara, S. R.; Silva, L. F. Exposure to polycyclic aromatic hydrocarbons in atmospheric $PM_{1.0}$ of urban environments: Carcinogenic and mutagenic respiratory health risk by age groups. *Environ. Pollut.* **2017**, *224*, 158−170.

(13) Moorthy, B.; Chu, C.; Carlin, D. J. Polycyclic aromatic hydrocarbons: from metabolism to lung cancer. *Toxicol. Sci.* **2015**, *145*, 5−15.

(14) Frenklach, M.; Wang, H.Detailed Modeling of Soot Particle Nucleation and Growth. In *Symposium (International) on Combustion*; Vol. 23; Elsevier, 1991; pp 1559−1566.

(15) Parker, D. S. N.; Kaiser, R. I.; Troy, T. P.; Ahmed, M. Hydrogen abstraction/acetylene addition revealed. *Angew. Chem. Int. Ed.* **2014**, *53*, 7740−7744.

(16) Yang, T.; Kaiser, R. I.; Troy, T. P.; Xu, B.; Kostko, O.; Ahmed, M.; Mebel, A. M.; Zagidullin, M. V.; Azyazov, V. N. HACA's heritage: A free-radical pathway to phenanthrene in circumstellar envelopes of asymptotic giant branch stars. *Angew. Chem. Int. Ed.* **2017**, *56*, 4515−4519.

(17) Zhao, L.; Kaiser, R. I.; Xu, B.; Ablikim, U.; Ahmed, M.; Joshi, D.; Veber, G.; Fischer, F. R.; Mebel, A. M. Pyrene synthesis in circumstellar envelopes and its role in the formation of 2D nanostructures. *Nat. Astron.* **2018**, *2*, 413−419.

(18) Kaiser, R. I.; Hansen, N. An Aromatic universe−A physical chemistry perspective. *J. Phys. Chem. A* **2021**, *125*, 3826−3840.

(19) Zhao, L.; Kaiser, R. I.; Xu, B.; Ablikim, U.; Ahmed, M.; Evseev, M. M.; Bashkirov, E. K.; Azyazov, V. N.; Mebel, A. M. Low-temperature formation of polycyclic aromatic hydrocarbons in Titan's atmosphere. *Nat. Astron.* **2018**, *2*, 973−979.

(20) Zhao, L.; Kaiser, R. I.; Xu, B.; Ablikim, U.; Ahmed, M.; Evseev, M. M.; Bashkirov, E. K.; Azyazov, V. N.; Mebel, A. M. A unified mechanism on the formation of acenes, helicenes, and phenacenes in the gas phase. *Angew. Chem. Int. Ed.* **2020**, *59*, 4051−4058.

(21) Zhao, L.; Kaiser, R. I.; Xu, B.; Ablikim, U.; Ahmed, M.; Zagidullin, M. V.; Azyazov, V. N.; Howlader, A. H.; Wnuk, S. F.; Mebel, A. M. VUV photoionization study of the formation of the simplest polycyclic aromatic hydrocarbon: Naphthalene ($C_{10}H_8$). *J. Phys. Chem. Lett.* **2018**, *9*, 2620−2626.

(22) Zhao, L.; Kaiser, R. I.; Xu, B.; Ablikim, U.; Lu, W.; Ahmed, M.; Evseev, M. M.; Bashkirov, E. K.; Azyazov, V. N.; Zagidullin, M. V.; et al. Gas phase synthesis of [4]-helicene. *Nat. Commun.* **2019**, *10*, 1510.

(23) Zhao, L.; Prendergast, M. B.; Kaiser, R. I.; Xu, B.; Ablikim, U.; Ahmed, M.; Sun, B. J.; Chen, Y. L.; Chang, A. H.; Mohamed, R. K.; Fischer, F. R. Synthesis of polycyclic aromatic hydrocarbons by phenyl addition−dehydrocyclization: The third way. *Angew. Chem. Int. Ed.* **2019**, *58*, 17442−17450.

(24) Jin, H.; Frassoldati, A.; Wang, Y.; Zhang, X.; Zeng, M.; Li, Y.; Qi, F.; Cuoci, A.; Faravelli, T. Kinetic modeling study of benzene and PAH formation in laminar methane flames. *Combust. Flame* **2015**, *162*, 1692−1711.

(25) Jin, H.; Xing, L.; Yang, J.; Zhou, Z.; Qi, F.; Farooq, A. Continuous Butadiyne addition to propargyl: A radical-efficient pathway for polycyclic aromatic hydrocarbons. *J. Phys. Chem. Lett.* **2021**, *12*, 8109−8114.

(26) Shao, C.; Wang, Q.; Zhang, W.; Bennett, A.; Li, Y.; Guo, J.; Im, H. G.; Roberts, W. L.; Violi, A.; Sarathy, S. M. Elucidating the polycyclic aromatic hydrocarbons involved in soot inception. *Commun. Chem.* **2023**, *6*, 223.

(27) Lieske, L.-A.; Commodo, M.; Martin, J. W.; Kaiser, K.; Benekou, V.; Minutolo, P.; D'anna, A.; Gross, L. Portraits of soot molecules reveal pathways to large aromatics, five-/seven-membered rings, and inception through π-radical localization. *ACS Nano* **2023**, *17*, 13563−13574.

(28) Adamson, B. D.; Skeen, S.; Ahmed, M.; Hansen, N. Detection of aliphatically bridged multi-core polycyclic aromatic hydrocarbons in sooting flames with atmospheric-sampling high-resolution tandem mass spectrometry. *J. Phys. Chem. A* **2018**, *122*, 9338−9349.

(29) Johansson, K. O.; Dillstrom, T.; Elvati, P.; Campbell, M. F.; Schrader, P. E.; Popolan-Vaida, D. M.; Richards-Henderson, N. K.; Wilson, K. R.; Violi, A.; Michelsen, H. A. Radical−radical reactions, pyrene nucleation, and incipient soot formation in combustion. *Proc. Combust. Inst.* **2017**, *36*, 799−806.

(30) Rundel, J. A.; Thomas, C. M.; Schrader, P. E.; Wilson, K. R.; Johansson, K. O.; Bambha, R. P.; Michelsen, H. A. Promotion of particle formation by resonance-stabilized radicals during hydrocarbon pyrolysis. *Combust. Flame* **2022**, *243*, No. 111942.

(31) Rundel, J. A.; Johansson, K. O.; Schrader, P. E.; Bambha, R. P.; Wilson, K. R.; Zádor, J.; Ellison, G. B.; Michelsen, H. A. Production of aliphatic-linked polycyclic hydrocarbons during radical-driven particle formation from propyne and propene pyrolysis. *Combust. Flame* **2023**, *258*, No. 112457.

(32) Agúndez, M.; Marcelino, N.; Cabezas, C.; Fuentetaja, R.; Tercero, B.; de Vicente, P.; Cernicharo, J. Detection of the propargyl radical at λ 3 mm. *Astro. Astrophys.* **2022**, *657*, A96.

(33) Johansson, K. O.; Head-Gordon, M.; Schrader, P.; Wilson, K.; Michelsen, H. Resonance-stabilized hydrocarbon-radical chain reactions may explain soot inception and growth. *Science* **2018**, *361*, 997−1000.

(34) Couch, D. E.; Zhang, A. J.; Taatjes, C. A.; Hansen, N. Experimental observation of hydrocarbon growth by resonance-stabilized radical-radical chain reaction. *Angew. Chem. Int. Ed.* **2021**, *60*, 27230−27235.

(35) Sinha, S.; Raj, A. Polycyclic aromatic hydrocarbon (PAH) formation from benzyl radicals: a reaction kinetics study. *Phys. Chem. Chem. Phys.* **2016**, *18*, 8120−8131.

(36) Kaiser, R. I.; Zhao, L.; Lu, W.; Ahmed, M.; Krasnoukhov, V. S.; Azyazov, V. N.; Mebel, A. M. Unconventional excited-state dynamics in the concerted benzyl (C_7H_7) radical self-reaction to anthracene ($C_{14}H_{10}$). *Nat. Commun.* **2022**, *13*, No. 786.

(37) Hirsch, F.; Constantinidis, P.; Fischer, I.; Bakels, S.; Rijs, A. M. Dimerization of the Benzyl radical in a high-temperature pyrolysis reactor investigated by IR/UV ion dip spectroscopy. *Chem. - Eur. J.* **2018**, *24*, 7647−7652.

(38) Sinha, S.; Rahman, R. K.; Raj, A. On the role of resonantly stabilized radicals in polycyclic aromatic hydrocarbon (PAH)

https://doi.org/10.1021/jacs.4c03417
J. Am. Chem. Soc. 2024, 146, 13571−13579

formation: pyrene and fluoranthene formation from benzyl-indenyl addition. *Phys. Chem. Chem. Phys.* **2017**, *19*, 19262−19278.
(39) Li, Y.; Cai, J.; Zhang, L.; Yuan, T.; Zhang, K.; Qi, F. Investigation on chemical structures of premixed toluene flames at low pressure. *Proc. Combust. Inst.* **2011**, *33*, 593−600.
(40) Jin, H.; Yang, J.; Xing, L.; Hao, J.; Zhang, Y.; Cao, C.; Pan, Y.; Farooq, A. An experimental study of indene pyrolysis with synchrotron vacuum ultraviolet photoionization mass spectrometry. *Phys. Chem. Chem. Phys.* **2019**, *21*, 5510−5520.
(41) Faccinetto, A.; Irimiea, C.; Minutolo, P.; Commodo, M.; D'Anna, A.; Nuns, N.; Carpentier, Y.; Pirim, C.; Desgroux, P.; Focsa, C.; Mercier, X. Evidence on the formation of dimers of polycyclic aromatic hydrocarbons in a laminar diffusion flame. *Commun. Chem.* **2020**, *3*, 112.
(42) Commodo, M.; Picca, F.; Vitiello, G.; De Falco, G.; Minutolo, P.; D'Anna, A. Radicals in nascent soot from laminar premixed ethylene and ehtylene-benzene flames by electron paramagnetic resonance spectroscopy. *Proc. Combust. Inst.* **2021**, *38*, 1487−1495.
(43) Jacobson, R. S.; Korte, A. R.; Vertes, A.; Miller, J. H. The molecular composition of soot. *Angew. Chem. Int. Ed.* **2020**, *59*, 4484−4490.
(44) Apicella, B.; Russo, C.; Carpentieri, A.; Tregrossi, A.; Ciajolo, A. PAHs and fullerenes as structural and compositional motifs tracing and distinguishing organic carbon from soot. *Fuel* **2022**, *309*, No. 122356.
(45) Marin, L. G.; Bejaoui, S.; Haggmark, M.; Svadlenak, N.; de Vries, M.; Sciamma-O'Brien, E.; Salama, F. Low-temperature formation of carbonaceous dust grains from PAHs. *Astrophys. J.* **2020**, *889*, 101.
(46) Fonfria, J. P.; Cernicharo, J.; Richter, M. J.; Lacy, J. H. A Detailed analysis of the dust formation zone of IRC + 10216 Derived from mid-infrared bands of C_2H_2 and HCN. *Astrophys. J.* **2008**, *673*, 445−469.
(47) Gielen, C.; Cami, J.; Bouwman, J.; Peeters, E.; Min, M. Carbonaceous molecules in the oxygen-rich circumstellar environment of binary post-AGB stars. *Astron. Astrophys.* **2011**, *536*, A54.
(48) Frisch, M. J.; Trucks, G. W.; Schlegel, H. B.; Scuseria, G. E.; Robb, M. A.; Cheeseman, J. R.; Scalmani, G.; Barone, V.; Petersson, G. A.; Nakatsuji, H.; Li, X.; Caricato, M.; Marenich, A. V.; Bloino, J.; Janesko, B. G.; Gomperts, R.; Mennucci, B.; Hratchian, H. P.; Ortiz, J. V.; Izmaylov, A. F.; Sonnenberg, J. L.; Williams-Young, D.; Ding, F.; Lipparini, F.; Egidi, F.; Goings, J.; Peng, B.; Petrone, A.; Henderson, T.; Ranasinghe, D.; Zakrzewski, V. G.; Gao, J.; Rega, N.; Zheng, G.; Liang, W.; Hada, M.; Ehara, M.; Toyota, K.; Fukuda, R.; Hasegawa, J.; Ishida, M.; Nakajima, T.; Honda, Y.; Kitao, O.; Nakai, H.; Vreven, T.; Throssell, K.; Montgomery, J. A., Jr.; Peralta, J. E.; Ogliaro, F.; Bearpark, M. J.; Heyd, J. J.; Brothers, E. N.; Kudin, K. N.; Staroverov, V. N.; Keith, T. A.; Kobayashi, R.; Normand, J.; Raghavachari, K.; Rendell, A. P.; Burant, J. C.; Iyengar, S. S.; Tomasi, J.; Cossi, M.; Millam, J. M.; Klene, M.; Adamo, C.; Cammi, R.; Ochterski, J. W.; Martin, R. L.; Morokuma, K.; Farkas, O.; Foresman, J. B.; Fox, D. J. *Gaussian 16, RC*; Gaussian, Inc.: Wallingford CT, 2016.
(49) Yu, H. S.; He, X.; Li, S. L.; Truhlar, D. G. MN15: A Kohn-Sham global-hybrid exchange-correlation density functional with broad accuracy for multi-reference and single-reference systems and noncovalent interactions. *Chem. Sci.* **2016**, *7*, 5032−5051.

https://doi.org/10.1021/jacs.4c03417
J. Am. Chem. Soc. 2024, 146, 13571−13579